Article

Discriminative Detection of Glutathione in Cell Lysates based on Oxidase-Like Activity of Magnetic Nanoporous Graphene

Haijuan Zhang, Jia Chen, Yali Yang, Li Wang, Zhan Li, and Hongdeng Qiu

Anal. Chem., **Just Accepted Manuscript** • DOI: 10.1021/acs.analchem.8b04779 • Publication Date (Web): 20 Mar 2019

Discriminative Detection of Glutathione in Cell Lysates based on Oxidase-Like Activity of Magnetic Nanoporous Graphene

Haijuan Zhang[‖], Jia Chen[‖], Yali Yang, Li Wang, Zhan Li, and Hongdeng Qiu*

CAS Key Laboratory of Chemistry of Northwestern Plant Resources/Key Laboratory for Natural Medicine of Gansu Province, Lanzhou Institute of Chemical Physics, Chinese Academy of Sciences, Lanzhou 730000, China

*Corresponding Author: Prof. Hongdeng Qiu, Fax: +86931 4968019; Tel: +86 931 4968877; E-mail: hdqiu@licp.cas.cn.

ABSTRACT: As the most abundant intracellular biothiol, glutathione (GSH) plays a central role in many cellular functions and has been proved to be associated with numerous clinical diseases. Nevertheless, it is still a challenge to detect GSH over other mercaptoamino-acids owing to their similar structures and activities. In this paper, magnetic nanoporous graphene (MNPG) nanocomposites were prepared for the first time through partial combustion of GO and ferric chloride. Due to combination of porous graphene and magnetic nanoparticles, the MNPG nanocomposites exhibited large specific surface area, fast mass and electron transport kinetics, resulting in remarkable mimic oxidase activity and easy separation. Based on the inhibition effect of GSH on the MNPG-catalyzed oxidation of thiamine, a novel and simple method for fluorescence determination of GSH was established. The sensor displayed a good linear response in the range of 0.2-20 μM towards GSH with a limit of detection of 0.05 μM. High sensitivity and selectivity facilitated its practical application for discriminative detection of GSH levels in PC12 cell lysates. The presented assay will enable a simple and powerful tool to monitor intracellular GSH levels for biomedical diagnosis. Furthermore, the MNPG nanocomposites will provide insights to construct nanoporous graphene based hybrids, and push forward the advancement of porous graphene for wide applications.

Glutathione (GSH), a thiol-containing tripeptide (γ-Glu-Cys-Gly), is the most abundant intracellular non-protein thiol and plays a pivotal role in maintaining redox homeostasis, combating oxidative stress, and defending against free radicals and toxins.[1,2] In particular, abnormal levels of cellular GSH have been closely associated with numerous clinical diseases, such as acquired immune deficiency syndrome (AIDS), cancer, heart problems, and neurodegenerative diseases.[3-5] Hence, the determination of cellular GSH level is critically important to better understand the role of GSH in biological systems, which is also of importance for accurate diagnosis of disease.

To date, various analytical techniques have been established for GSH detection, such as high performance liquid chromatography (HPLC), mass spectrometry, electrochemistry, and immunoiluminescence, etc.[6-10] Though most of these approaches exhibit high sensitivity, they suffer from non-negligible intrinsic shortcomings such as expensive instruments, time-consuming operation process, or complicated synthetic procedures. Spectrometry has emerged as the most convenient and promising tool for GSH detection owing to its operational simplicity, inexpensive cost and high sensitivity. However, discriminative detection of GSH over cysteine (Cys) and homocysteine (Hcy) remains a tough task because of their similar structures and reactivity. Therefore, it is still highly desired to develop facile GSH sensing approaches with high sensitivity and selectivity to meet the biological and clinical requirements.

In recent years, nanomaterial-based enzyme mimics (nanozymes) have been broadly investigated as new artificial enzymes towing to their remarkable properties including easy synthesis, good stability, low cost, and design flexibility, in comparison with those of natural enzymes.[11-13] So far, efforts have been made to explore nanozymes materials for GSH detection, such as Fe_3O_4 nanoparticles,[14] manganese oxides,[15] graphene dots,[16] Au nanoparticles,[17] metal organic frameworks,[18] and so on. Nevertheless, poor diffusion and low catalytic activity of those nanozymes restrict the applications in biological media. In order to address these drawbacks, the construction of enzyme mimics materials with outstanding diffusion and high catalytic activity is urgently needed.

Two-dimensional (2D) nanoporous graphene (NPG) has attracted vast interests recently due to their extraordinary physiochemical properties such as unique porous structures, large surface area and excellent electronic conductivity.[19] The unordinary features facilitate the widely applications of NPG in electrochemical capacitors, field effect transistors (FETs), sensors, separation science and molecular sieving.[20-24] Moreover, the nanopores on the graphene sheets can effectively impede aggregation of intersheets, accelerate mass transfer and electron diffusion.[25,26] Combining the advantages from individual components, NPG-based hybrid materials may possess synergistic effects, resulting in enhanced catalytic activity of NPG-based nanocomposites. Magnetic nanoparticles (NPs) have received considerable attention on account of their remarkable properties of large surface-to-volume ratio and superparamagnetism. The integration of NPG and magnetic NPs into magnetic nanoporous graphene (MNPG) nanocomposites may produce new and/or enhanced performance that cannot be realized by either component alone, resulting in potential applications in many fields. Though the assembly of magnetic NPs on graphene oxide has been

reported,[27,28] integrating the magnetic NPs and NPG nanocomposite has rarely been reported to date, which is probably ascribed to the limitation in synthetic approach and the difficulty in fabrication of high quality NPG-based hybrids.

In our recent work, we proposed a simple and rapid method for the preparation of porous graphene by partial combustion of graphene oxide imperfectly covered by hydrotalcite.[29] Enlightened by this previous study, we suppose that different kinds of NPG/metal oxide nanocomposites could be achieved by changing the salt precursors. Herein, we for the first time proposed a new and simple approach to fabricate MNPG nanocomposites through combustion reaction of graphene oxide (GO) and $FeCl_3$. Expectedly, the as-prepared MNPG nanocomposites exhibit outstanding catalytic activity and could be applied for sensitive and discriminative determination of GSH in cell lysates.

EXPERIMENTAL SECTION

Materials and Chemicals. Graphite powder and H_2O_2 were obtained from Sigma-Aldrich Chemical Co. (St. Louis, MO, USA). Quantitative filter paper (12.5 cm) was bought from Sinopharm Chemical Reagent Co. Ltd., China. GO was prepared from graphite powder by a well-known Hummer's method with some modifications.[30] $FeCl_3 \cdot 6H_2O$, HCl, H_2SO_4, $NaNO_3$, $KMnO_4$ and vitamin B1 (also named thiamine, TH) were purchased from Aladdin Chemistry Co. Ltd. (Shanghai, China). L-Cysteine (L-Cys), L-lysine (L-Lys), L-arginine (L-Arg), L-ascorbic acid (L-AA), L-histidine (L-His), L-methionine (L-Met), L-tyrosine (L-Tyr), L-tryptophan (L-Trp), L-phenylalanine (L-Phe), homocysteine (Hcy), L-isoleucine (L-Ile), L-threonine (L-Thr), L-alanine (L-Ala), L-serine (L-Ser), L-valine (L-Val), L-glycine (L-Gly), glucose, catechol, nicotinamide adenine dinucleotide phosphate (NADPH), nicotinamide adenine dinucleotide (NADH) and glutathione (GSH) were bought from Sangon Biological Engineering Technology & Services Co., Ltd (Shanghai, China). Dialysis membrane with a molecular weight cut off of 8000-14000 $g \cdot mol^{-1}$ was purchased from Beijing Chemical Reagent Co., Ltd (Beijing, China). PC12 cells (neuron-like rat pheochromocytoma cell line) were obtained from Shanghai Institute of Biochemistry and Cell Biology, Chinese Academy of Sciences. Dulbecco's Modified Eagle Medium (DMEM) was purchased from Sigma-Aldrich (St. Louis, USA). All reagents were of analytical grade and used as received without any further purification. All aqueous solutions were prepared with ultrapure water of resistivity not less than 18.2 MH cm (Milli-Q plus 185 equip, USA).

Apparatus and Characterizations. Transmission electron microscopy (TEM) and energy dispersive X-ray spectrum (EDX) were performed with a Tecnai G2 TF20 transmission electron microscope (FEI, USA). Fourier transform infrared spectrum (FT-IR) was conducted on an IFS 120HR Fourier transform infrared spectrometer (Bruker, Germany). X-Ray diffraction (XRD) patterns were observed by means of X ′ Pert PRO X-ray diffractometer (PANalytical, Netherlands). X-ray photoelectron spectroscopy (XPS) analyses were recorded on an ESCALAB 250Xi spectrometer (ThermoFisher Scientific, USA). The magnetic property of MNPG nanocomposites was measured with a vibrating sample magnetometer (VSM, Lakeshore Cryotronics 730, USA) at room temperature. The content of Fe in MNPG nanocomposite was 25.4% as determined by inductively coupled plasmas atomic emissive spectrometry (ICP-AES, IRIS Advantage ER/S, TJA). High resolution mass spectrum (HRMS) of reaction product was recorded on a MicroTof Q II (Bruker, USA). Raman spectra were explored with a laser scanning confocal micro-Raman spectrometer (LabRAM HR Evolution, HORIBA, France), and the samples were scanned in an extended range of 100 to 4000 cm^{-1}. Fluorescence (FL) spectra were measured using a LS-55 fluorescence spectrometer (Perkin-Elmer, USA) with a 1 mL quartz cuvette (1 cm optical path). The FL spectra of the solution were recorded in the wavelength of 400-600 nm.

Preparation of MNPG. The nanocomposite of NPG and ferric oxide was prepared through combustion reaction. In brief, 1.0 g $FeCl_3 \cdot 6H_2O$ was mixed with a solution of GO (1.0 mL, 5.0 $mg \cdot mL^{-1}$) under continuous sonication for 1 h. Then the mixture was filtered through quantitative filter paper so that most of GO and a certain amount of $FeCl_3$ would be trapped together on the filter paper. The filter paper covered by GO and $FeCl_3$ was dried in vacuum oven at 60 °C. After the temperature of the muffle furnace reached 450 °C, the covered filter paper was placed on a tin foil and put into the muffle furnace with tongs and ignited at 450 °C for 2 min (timed with a stopwatch). Then the sheets on the tin foil was taken out with tongs carefully and naturally cooled to room temperature. Finally, the collected sheets were washed and centrifuged with ultrapure water for 10 times to remove unreacted $FeCl_3$ and other residual impurities (until the supernatant becomes colorless). At last, the product was washed with ethanol and dried at 60 °C overnight. The resultant composites were named as MNPG. Pure NPG can be easily obtained by washing MNPG with diluted hydrochloric acid.[29]

Preparation of PC12 cell lysates samples. PC12 cells were cultured in DMEM medium (10% FBS, 2 mM glutamine, and 100 units·mL^{-1} penicillin/streptomycin). To prepare PC12 cell lysates samples, the cells were harvested and resuspended using KPE buffer (0.1% TritonX-100 and 0.6% sulfosalicyclic acid in 0.1 M potassium phosphate buffer with 5 mM EDTA, pH 7.5). Then the suspension was sonicated for 2-3 min, followed by centrifugation at 3000 g for 4 min at 4 °C. The obtained supernatant was ready for GSH assay. The first panel was served as a vehicle control. For comparison, the other two panels were pretreated with 6-hydroxydopamine and thioctamide, respectively. Other experimental procedures were the same as above-mentioned.

Detection of GSH in cell lysates samples. The determination of GSH in the PC12 cell lysates was carried out as follows: 710 μL of phosphate buffer solution (10 mM, pH=12.0), 150 μL of MNPG nanocomposite (1 $mg \cdot mL^{-1}$), and 40 μL of 20 mM TH were mixed with 100 μL varied concentrations of GSH (with final concentrations of 0, 0.2, 0.5, 2, 4, 10, 20, 40 and 60 μM). Subsequently, the mixtures were vibrated at 40 ºC for 5 min to allow the oxidative reaction of TH. The generated fluorescence intensity at 445 nm was recorded immediately. The concentrations of GSH in the PC12 cell lysates samples were estimated by using the standard addition method. All the experiments were repeated for three times.

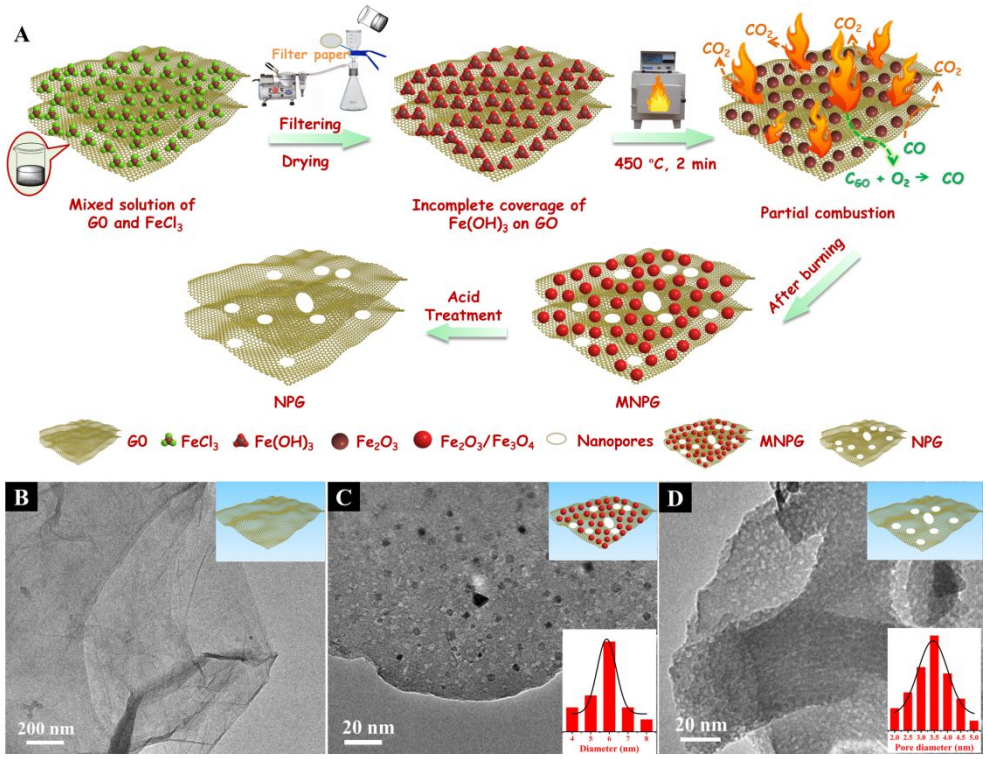

Figure 1. Schematic illustration for the combustive synthesis processes of MNPG and NPG (A) and TEM images of GO (B), MNPG nanocomposite (C) and NPG (D). Insets are the size distribution of the magnetic NPs (inset of C) and the nanopores (inset of D), which are calculated from 50 individual particles and nanopores, respectively.

RESULTS AND DISCUSSION

Characterizations of MNPG. The process for preparing MNPG from GO and ferric chloride under combustive treatment was schemed in **Figure 1A**. Firstly, GO was added to a high concentration solution of $FeCl_3$. After sonicated to disperse, the mixture was filtered through quantitative filter paper, then a certain amount of GO and $FeCl_3$ was trapped on the filter paper. During the heating and drying process, the Fe^{3+} ions were hydrolyzed to form $Fe(OH)_3$,[31] leading to the incomplete coverage of $Fe(OH)_3$ layer on the surface of GO. By igniting, thermally stressed $Fe(OH)_3$ would decompose into α-Fe_2O_3, which could be served as template and precursors.[31,32] During the process of carbothermal reduction, GO served as the reducing agent and carbon source (C_{GO}). At a high reaction temperature, the bare GO in uncovered region would be burned, while the α-Fe_2O_3 were partially reduced to Fe_3O_4, resulting in the resultant products.[33] The TEM was performed to characterize the morphological and structural features of the samples. **Figure 1B** and **1C** showed the TEM images of GO and the resultant MNPG nanocomposite after combustive treatment, respectively. As can be seen, numerous nanoparticles were uniformly distributed on the graphene sheet ($\approx$ 6.5 nm). The EDX spectrum indicated that the nanoparticles were composed of iron oxide (**Figure S1**). Along with these nanoparticles, some nanopores also could be observed on the surface of graphene with an average pore size of $\approx$ 3.5 nm, giving clear evidence for the successful preparation of MNPG nanocomposites. After washing out the iron oxide particles with dilute hydrochloric acid, the porous structure of NPG could be clearly observed (**Figure 1D**), further proving the existence of nanopores in the composites.

The crystallinity of pure NPG and MNPG nanocomposites was investigated by X-ray diffractometer, as presented in **Figure 2A**. Compared with the XRD pattern of GO (**Figure S2A**), the (001) crystal planes at 10.9º of GO nanosheet disappeared, while the (002) crystal planes at 21.2º were found in NPG and MNPG. The broad diffraction peak at 21.2º was indexed to the irregular stacking of the NPG sheets. The diffraction peak of iron oxide phases could also be identified by XRD. The strong and sharp peaks appeared within 0-80° indicated the existence of α-Fe_2O_3 and Fe_3O_4 crystalline phases. The peaks and corresponding indexed planes appeared at 30.04° (220), 35.44° (311), 43.03° (400), 54.03° (422), 56.95° (511), and 62.89° (440) matched well with magnetite (JCPDS file No. 75-0033), which confirmed the existence of Fe_3O_4.[34] The peaks and corresponding indexed planes appeared at 24.08° (012), 33.07° (104), 35.44° (110), 40.78° (113), 49.38° (024), 54.03° (116), 62.48° (214), and 64.01° (300) matched hematite (α-Fe_2O_3) (JCPDS file No. 33-0664).[35] To further verify the existence of α-Fe_2O_3 and Fe_3O_4, magnetic hysteresis loop of the composites was recorded by a VSM with an applied field sweeping from -20 to 20 *k*Oe (**Figure 2B**). The magnetic hysteresis curve showed the reversible behavior and nonlinear between the applied magnetic field and the magnetization. With the increasing of applied magnetic field, the magnetization tended to be saturated with an *Ms* value of 3.6 emu·g^{-1}, which facilitated the magnetic separation in practical manipulation. On the basis of the XRD and VSM results, we know that the nanoparticle features of this hybrid material were α-Fe_2O_3 and Fe_3O_4.

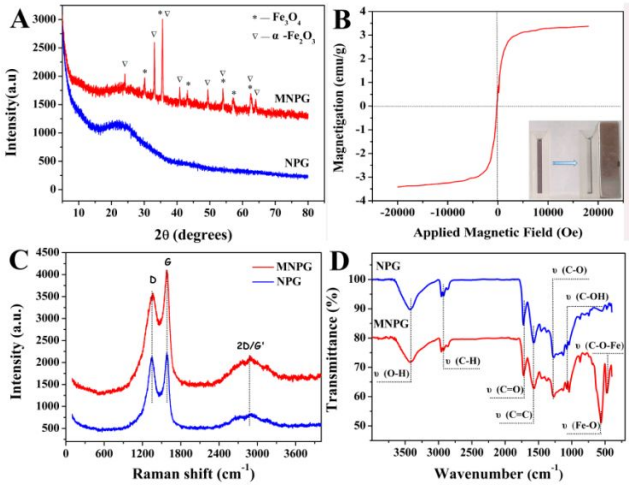

Figure 2. (A) XRD patterns of the resultant NPG and MNPG, (B) magnetic hysteresis loops of MNPG, (C) Raman spectra and (D) FT-IR spectra of the as-synthesized NPG and MNPG.

Raman spectroscopy was also applied for further characterization of the nanocomposite. The Raman spectrum of GO revealed a D bond at 1361 cm^{-1}, a G bond at 1602 cm^{-1} and a 2D/G' bond at about 2720 cm^{-1} (**Figure S2B**). The G band is ascribed to an E_{2g} mode of graphite related to the vibration of sp^2 bonded carbon atoms, the D band peak is associated with the structural defect or partially disordered graphite domains, whereas the 2D/G' bond is a second-order two-phonon mode.[36] After the combustive treatment, the intensity ratio (I_D/I_G) decreased from 1.04 for pristine GO to 0.93 for NPG (**Figure 2C**). The decreasing D peak of Raman shift indicated that high crystalline porous graphene could be obtained after combustive treatment.[37] The removal of oxygen defects would render a much higher content of sp^2 carbon, which was indicated by a significantly increased G band peak. Decreasing of I_D/I_G ratio indicated that the combustive of GO could effectively remove the oxygen defects and partially rebuild the sp^2 network of graphene.[38]

Figure 2D showed the FT-IR spectra of NPG and MNPG. The peak at 3200-3500 cm^{-1} was from stretching vibrations of O-H. The band at 2938 cm^{-1} was assigned to the bending vibration of C-H. The absorption bands at 1575 and 1715 cm^{-1} were attributed to the stretching vibrations of C=C in benzene ring and C=O of carboxylic acid, respectively, which were corresponding to the graphene structure. The bands at 490 and 520 cm^{-1} were from C-O-Fe and Fe-O stretching vibrations, confirming the formation of magnetic porous graphene composites.

Surface sensitive XPS reveals more information with regard to the surface composition and the chemical states of elements in MNPG nanocomposites. The full range XPS (**Figure 3A**) clearly showed three peaks at 285.9, 532.0, and 710.0 eV, which were attributed to C 1s, O 1s and Fe 2p, respectively.[39] In C 1s spectrum (**Figure 3B**), the fitted peaks at 284.6, 285.0, 286.4, and 288.7 eV were assigned to C=C (sp^3), C-C (sp^3), C-O (sp^2), and O-C=O (sp^2) groups, respectively.[40] In O 1s spectrum (**Figure 3C**), the peaks at 532.5 and 533.6 eV were assigned to C=O and C-O bonds, respectively.[41] The peak about 530.3 eV was assigned to the oxygen in Fe-O,[42] and the peak located at 531.6 eV should be caused by the bond of Fe-O-C formed between Fe_3O_4 and graphene.[43] As shown

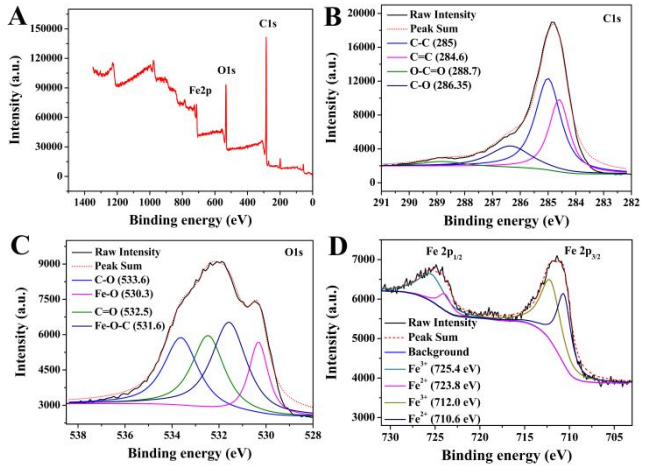

Figure 3. The wide-survey XPS spectrum (A) and high-resolution C1s (B), O1s (C) and Fe2p (D) XPS spectrum of MNPG.

in **Figure 3D**, the high resolution spectrum of Fe 2p had character istic Fe $2p_{3/2}$ and Fe $2p_{1/2}$ doublets of iron oxide electrons. The Fe 2p peaks fitted well with the 2p sub shells of Fe^{3+} and Fe^{2+}, confirming the existence of Fe^{2+} and Fe^{3+} in the nanocomposites.[35] The peaks at 712.0 and 725.4 eV corresponded to the Fe^{3+} in α-Fe_2O_3.[44] The peaks at 710.6 and 723.8 eV were related to the Fe^{2+} in Fe_3O_4. [45] XPS measurements further proved the formation of α-Fe_2O_3 and Fe_3O_4, which was in good agreement with the XRD results. The relative atomic ratio of Fe^{3+}/Fe^{2+} (γ) could be calculated according to the following equation[32]:

$$\frac{n_i}{n_j} = \frac{I_i}{I_j}\sqrt{\frac{E_{kj}}{E_{ki}}}$$

where n_i and n_j represent the number of surface atoms, I_i and I_j represent the peak areas, and E_{kj} and E_{ki} represent the photoelectron kinetic energies. According to the peak areas of Fe^{2+} and Fe^{3+} (**Figure 3D**), γ was estimated to be 2.24. Furthermore, the total content of Fe among the nanocomposite was determined to be 25.4% by ICP-AES. Accordingly, the mass fraction of α-Fe_2O_3 and Fe_3O_4 in MNPG were 14.0% and 32.3%, respectively, with a ratio of 3:5. After washing out the iron oxide with dilute HCl, pure NPG could be obtained, accompanied by the disappearance of Fe 2p peaks (**Figure S3**). Both XRD and XPS confirmed the successful preparation of NPG and MNPG nanocomposites.

Mimick oxidase application of MNPG for detection of GSH. It have been reported that Fe_3O_4 and GO exhibit properties mimicking those of enzymes.[46,47] These findings motivate our curiosity to investigate the mimic enzyme activity of MNPG because of the combination of Fe_3O_4 and NPG. TH, a non-fluorescent compound, can be easily converted to strong fluorescent thiochrome (TC) in basic media by appropriate oxidants.[48] Thus TH can also act as an attractive fluorescent substrate for oxidative detection. In the present work, the as-prepared nanocomposite could catalyze the oxidation of TH, resulting in the generation of fluorescence (the reaction scheme was given in **Figure 4A**). **Figure S4A** depicted the FL response of the sensing system by using different materials as catalysts. The system containing only TH exhibited almost none FL intensity. After Fe_3O_4 or NPG was added, the FL intensity of the solution was enhanced

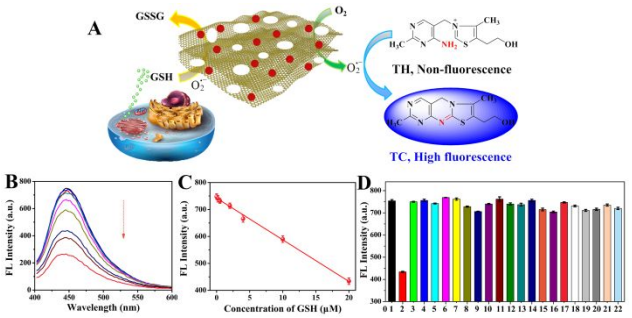

Figure 4. (A) Schematic illustration of the MNPG-based fluorescent assay for GSH detection. (B) Fluorescence emission spectra of TH upon the addition of various concentrations of GSH (from top to bottom, 0, 0.2, 0.5, 2, 4, 10, 20, 40, and 60 μM). (C) The linear calibration curve of GSH with X-axis representing different concentrations of GSH ranging from 0.2-20 μM and Y-axis representing their corresponding fluorescence intensity at 445 nm. (D) Fluorescence response of the system toward GSH (20 μM) and other interferents with the concentrations of 200 μM (3-18) and 2 μM (19-22): 1, control; 2, GSH, 3, L-Trp, 4, L-His, 5, L-Met, 6, L-Arg, 7, L-Lys, 8, L-Tyr, 9, L-Cys, 10, Hcy, 11, L-Phe, 12, L-Ile, 13, L-Thr, 14, L-Ala, 15, L-Ser, 16, L-Val, 17, L-Gly, 18, glucose, 19, L-AA, 20, catechol, 21, NADPH, 22, NADH. Error bars represent the standard deviation of three repeated measurements.

to a certain extent, while significant enhancement was obtained after the addition of MNPG nanocomposite, implying the higher oxidase-like activity of MNPG nanocomposite compared to that of Fe_3O_4 and NPG. The high catalytic activity of MNPG may be contributed to the following factors: (1) the 3D architectures of NPG could provide high surface area as well as fast mass and electronic transfer kinetics because of the combination of the porous structures and excellent intrinsic character of graphene;[25-26] (2) Fe_3O_4 could reduce the aggregation of graphene layers;[49] (3) synergetic effects between NPG and Fe_3O_4 in nanocomposite. On one hand, the electrons involved in the carbon network of NPG could donate electrons to reduce O_2 *via* electron transfer. The use of NPG "support" could provide abundant active sites and greatly improve the stability and dispersion of Fe_3O_4 to allow for better distribution.[50] On the other hand, the Fe_3O_4 on the graphene sheets could also serve as electron carrier during electron transfer.[51] Moreover, Fe_3O_4 could effectively impede aggregation of graphene intersheets, accelerate mass transfer and electron diffusion. Collectively, these results may in turn facilitate significantly enhanced oxidase-like activities of the MNPG nanocomposite.

The BET surface area and average pore diameter of MNPG (419 m^2/g, 3.4 nm) were lower than that of NPG (482 m^2/g, 3.5 nm), as shown in **Figure S5**. This could be due to the filling or blocking of the surface and pores in NPG by α-Fe_2O_3 and Fe_3O_4 nanoparticles, resulting in a lower surface area and pore diameter.

Some important factors affecting the fluorescence spectra of the system were investigated, including the effect of TH and MNPG concentration, pH values, reaction time and temperature (**Figure S4B-4F**). Subsequently, oxidase-mimicking activity of the MNPG nanocomposite was investigated according to steady-state kinetic analysis. The apparent kinetic parameters were calculated according to the function: $\upsilon = V_{max} \times [S]/(K_m + [S])$, where υ represents the initial velocity, V_{max} represents the maximum reaction velocity, $[S]$ represents the substrate concentration, and K_m represents the Michaelis constant that reflects the affinity of the enzyme for the substrate. [51] As illustrated in **Figure S6**, the apparent values of K_m and V_{max} were 120.8 μM and 212.8 nM s^{-1}, respectively. The K_m value of MNPG with TH is much lower than that of the natural horseradish peroxidase (HRP, K_m = 434 μM), Acr^+-Mes (129 μM) and fluorescein (K_m =158 μM), illustrating the higher oxidase-like activity of MNPG nanocomposite. [52-54]

Based on the above excellent properties of the MNPG nanocomposite, a novel and simple sensing approach was fabricated for GSH detection. **Figure 4B** depicted the FL spectra of TC after the addition of varied concentrations of GSH. Initially, the non-fluorescent TH was oxidized to TC under the optimum conditions, resulting in high fluorescence. After adding varied concentrations of GSH, the FL intensity at 445 nm gradually decreased. As it is known that GSH could be oxidized into glutathione disulfide (GSSG), [55] which could also be verified in **Figure S7**. The competing oxidation of GSH and TH restrained the oxidation of TH, leading to the decrease of fluorescent after the introduction of GSH. The gradual decrease of FL intensity revealed the sensitivity of the system towards GSH concentration. As shown in **Figure 4C**, there displayed a good linearity between the fluorescent of TC versus the concentration of GSH ranging from 0.2 to 20 μM. The limit of detection (LOD, calculated by 3σ/S, where σ represents the standard deviation of blank signal, and S represents the slope of the calibration curve) was 0.05 μM, which was comparable with or even better than other fluorescent or mimic enzymes-based methods (**Table S1**).[4, 15-17, 53, 56-63]

The intracellular complexity possesses a great challenge for the detection of GSH. Taking into account that the mercaptoamino acids coexist in biological fluids, it is more difficult to discriminate GSH from Cys/Hcy. Thus the influence of a series of biologically relevant amino acids (especially L-Cys and Hcy) and some other reductive species (glucose, L-AA, catechol, NADPH and NADH) were evaluated. As shown in **Figure 4D**, only GSH induced effective fluorescence reduction under the optimal conditions. In stark contrast, neither L-Cys nor Hcy displayed fluorescence interference at 445 nm. As GSH is the most abundant intracellular reductive small molecule, its level is much higher than the other reductive species.[16] To better simulate the intracellular condition, a concentration of 2 μM was utilized for other reductive species. In this case, Glucose, L-AA, catechol, NADPH and NADH were also negative to the probe. Collectively, the proposed method possessed high selectivity for GSH and could address the biological requirements.

In virtue of the analytical advantages, the MNPG-based sensor was also utilized for GSH detection in complicated biological samples. As is reported, GSH is the most abundant intracellular antioxidant for many mammalian. Besides, more than 90% of the intracellular thiol molecule is GSH in most cell samples. Here, PC12 cell was chosen as the model cancer cell. Thioctamide was utilized as the stimulant agent in order to induce GSH generation from cancer cells, and 6-hydroxydopamine was used to reduce GSH generation. As displayed in **Table 1**, a standard addition method was used by spiking different concentrations of GSH into PC12 cell lysates. The GSH level in the control cell lysates sample was determined to be 0.40 mM, which was close to the normal concentration of GSH in cells (0.5-10 mM).[16] In order to

Table 1. Determination of GSH in PC12 cell lysates samples.

Samples	Detected (μM)	Added (μM)	Found (μM)	Recovery (%)	RSD (%)
Normal PC12 cell lysates	399.3	5.0	404.0	94.0	6.3
		10.0	409.9	106.0	1.9
		20.0	420.0	103.5	2.8
Pretreated with 6-hydroxydopamine	331.4	5	336.0	92.0	5.2
		10	340.8	94.0	3.2
		20	351.7	101.5	3.6
Pretreated with thoctamide	451.1	5	456.3	104.0	4.8
		10	460.6	95.0	3.7
		20	470.5	97.0	5.4

confirm the feasibility of the proposed method, we carried out other experiments by pretreating the PC12 cells with thioctamide and 6- hydroxydopamine, respectively, to change the GSH levels in cell lysates. As expected, the concentration of GSH in cell lysates pretreated with thioctamide increased to 0.45 mM, while the one pretreated with 6-hydroxydopamine decreased to 0.33 mM. These results together suggested that the proposed method was suitable for detecting GSH levels in cell lysates. Furthermore, the recoveries of given amount of GSH in cell lysates samples were ranged from 92.0% to 106.0%, and the RSDs were ranged from 1.9% to 6.3%. The satisfactory recoveries and RSDs definitely implied high accuracy and reliability of the established method for the detection of GSH in biological samples.

CONCLUSIONS

In summary, for the first time, a simple and rapid method to fabricate MNPG nanocomposites was developed by partial combustion of GO and ferric chloride. Combining the advantages from both nanoporous graphene and magnetic NPs, the MNPG nanocomposites possess high specific surface area as well as fast mass and electron transport kinetics, resulting in remarkable catalytic activity and easy separation. On the basis of their mimic oxidase activity, the MNPG nanocomposites have been successfully applied for discriminative detection of GSH levels in PC12 cell lysates with high sensitivity and selectivity. More notably, our strategy will open new avenues for the fabrication of nanoporous graphene based hybrids, but also inspire more brilliant work in the future, and pave the way for the advancement of porous graphene for a variety of applications.

ASSOCIATED CONTENT

Supporting Information

The Supporting Information is available free of charge on the ACS Publications website.

EDX of the MNPG nanocomposite, XRD pattern and raman spectrum of GO, survey XPS and high-resolution C1s, O1s spectrum of NPG, nitrogen sorption isotherms and pore size distribution curves of NPG and MNPG, fluorescence emission spectra of TC upon the addition of variable materials, optimization of variable experimental factors, steady-state kinetic assay and Lineweaver-Burk plot of MNPG, high resolution mass spectrum of the reaction solution and comparison of analytical performance with other methods.

AUTHOR INFORMATION

Author Contributions

[I]These two authors contributed equally to this work.

Notes

There are no conflicts of interest to declare.

ACKNOWLEDGMENT

The authors gratefully acknowledge the financial support provided by the National Natural Science Foundation of China (21822407, 21675164), the Natural Science Foundation of Gansu Province (17JR5RA311, 18JR3RA387) and CAS "Light of West China" Program.

REFERENCES

[1] Li, H.; Peng, W.; Feng, W.; Wang, Y.; Chen, G.; Wang, S.; Li, S.; Li, H.; Wang, K.; Zhang, J. A novel dual-emission fluorescent probe for the simultaneous detection of H_2S and GSH. *Chem.Commun.* **2016**, 52, 4628-4631.

[2] Miller, E. W.; Bian, S. X.; Chang, C. J. A Fluorescent Sensor for Imaging Reversible Redox Cycles in Living Cells. *J. Am. Chem. Soc.* **2007**, 129, 3458-3459.

[3] Zhang, Y.; Shao, X.; Wang, Y.; Pan, F.; Kang, R.; Peng, F.; Huang, Z.; Zhang, W.; Zhao, W. Dual emission channels for sensitive discrimination of Cys/Hcy and GSH in plasma and cells. *Chem.Commun.* **2015**, 51, 4245-4248.

[4] Ni, P.; Sun, Y.; Dai, H.; Hu, J.; Jiang, S.; Wang, Y.; Li, Z. Highly sensitive and selective colorimetric detection of glutathione based on Ag [I] ion–3,3′,5,5′-tetramethylbenzidine (TMB). *Biosens. Bioelectron.* **2015**, 63, 47-52.

[5] Shi, Y.; Pan, Y.; Zhang, H.; Zhang, Z.; Li, M.-J.; Yi, C.; Yang, M. A dual-mode nanosensor based on carbon quantum dots and gold nanoparticles for discriminative detection of glutathione in human plasma. *Biosens. Bioelectron.* **2014**, 56, 39-45.

[6] Tcherkas, Y. V.; Denisenko, A. D. Simultaneous determination of several amino acids, including homocysteine, cysteine and glutamic acid, in human plasma by isocratic reversed-phase high-performance liquid chromatography with fluorimetric detection. *J. Chromatogr. A* **2001**, 913, 309-313.

[7] Burford, N.; Eelman, M. D.; Mahony, D. E.; Morash, M. Definitive identification of cysteine and glutathione complexes of bismuth by mass spectrometry: assessing the biochemical fate of bismuth pharmaceutical agents. *Chem.Commun.* **2003**, 146-147.

[8] Zhu, W.; Jiang, G.; Xu, L.; Li, B.; Cai, Q.; Jiang, H.; Zhou, X. Facile and controllable one-step fabrication of molecularly imprinted polymer membrane by magnetic field directed self-assembly for electrochemical sensing of glutathione. *Anal. Chim. Acta* **2015**, 886, 37-47.

[9] Wawegama, N. K.; Browning, G. F.; Kanci, A.; Marenda, M. S.; Markham, P. F. Development of a Recombinant Protein-Based Enzyme-Linked Immunosorbent Assay for Diagnosis of Mycoplasma bovis infection in cattle. *Clin. Vaccine Immunol.* **2014**, 21, 196-202.

[10] Qi, S.; Liu, W.; Zhang, P.; Wu, J.; Zhang, H.; Ren, H.; Ge, J.; Wang, P. A colorimetric and ratiometric fluorescent probe for highly selective detection of glutathione in the mitochondria of living cells. *Sens. Actuat. B* **2018**, 270, 459-465.

[11] Xie, J.; Zhang, X.; Wang, H.; Zheng, H.; Huang, Y.; Xie, J. Analytical and environmental applications of nanoparticles as enzyme mimetics. *TRAC-Trend Anal. Chem.* **2012**, 39, 114-129.

[12] Lin, Y.; Ren, J.; Qu, X. Catalytically Active Nanomaterials: A Promising Candidate for Artificial Enzymes. *Accounts Chem. Res.* **2014**, 47, 1097-1105.

[13] Wei, H.; Wang, E. Nanomaterials with enzyme-like characteristics (nanozymes): next-generation artificial enzymes. *Chem. Soc. Rev.* **2013**, 42, 6060-6093.

[14] Liu, S.; Lu, F.; Xing, R.; Zhu, J.-J. Structural Effects of Fe_3O_4 Nanocrystals on Peroxidase-Like Activity. *Chem. Eur. J.* **2011**, 17, 620-625.

[15] Zhang, X.; Mao, X.; Li, S.; Dong, W.; Huang, Y. Tuning the oxidase mimics activity of manganese oxides via control of their growth conditions for highly sensitive detection of glutathione. *Sens. Actuat. B* **2018**, 258, 80-87.

[16] Zheng, A.-X.; Cong, Z.-X.; Wang, J.-R.; Li, J.; Yang, H.-H.; Chen, G.-N. Highly-efficient peroxidase-like catalytic activity of graphene dots for biosensing. *Biosens. Bioelectron.* **2013**, 49, 519-524.

[17] Kumar, V.; Bano, D.; Singh, D. K.; Mohan, S.; Singh, V. K.; Hasan, S. H. Size-Dependent Synthesis of Gold Nanoparticles and Their Peroxidase-Like Activity for the Colorimetric Detection of Glutathione from Human Blood Serum. *ACS Sustain. Chem. Eng.* **2018**, 6, 7662-7675.

[18] Zhang, Y.; Zhang, W.; Chen, K.; Yang, Q.; Hu, N.; Suo, Y.; Wang, J. Highly sensitive and selective colorimetric detection of glutathione via enhanced Fenton-like reaction of magnetic metal organic framework. *Sens. Actuat. B* **2018**, 262, 95-101.

[19] Han, S.; Wu, D.; Li, S.; Zhang, F.; Feng, X. Porous Graphene Materials for Advanced Electrochemical Energy Storage and Conversion Devices. *Adv. Mater.* **2014**, 26, 849-864.

[20] Zeng, Z.; Huang, X.; Yin, Z.; Li, H.; Chen, Y.; Li, H.; Zhang, Q.; Ma, J.; Boey, F.; Zhang, H. Fabrication of Graphene Nanomesh by Using an Anodic Aluminum Oxide Membrane as a Template. *Adv. Mater.* **2012**, 24, 4138-4142.

[21] Li, Z.; Liu, Y.; Zhao, Y.; Zhang, X.; Qian, L.; Tian, L.; Bai, J.; Qi, W.; Yao, H.; Gao, B.; Liu, J.; Wu, W.; Qiu, H. Selective Separation of Metal Ions via Monolayer Nanoporous Graphene with Carboxyl Groups. *Anal. Chem.* **2016**, 88, 10002-10010.

[22] Liu, Y.; Liu, X.; Guo, Z.; Hu, Z.; Xue, Z.; Lu, X. Horseradish peroxidase supported on porous graphene as a novel sensing platform for detection of hydrogen peroxide in living cells sensitively. *Biosens. Bioelectron.* **2017**, 87, 101-107.

[23] Song, L.; Zhang, H.; Cai, T.; Chen, J.; Li, Z.; Guan, M.; Qiu, H. Porous graphene decorated silica as a new stationary phase for separation of sulfanilamide compounds in hydrophilic interaction chromatography. *Chinese Chem. Lett.* **2018**, doi: 10.1016/j.cclet.2018.10.040.

[24] Celebi, K.; Buchheim, J.; Wyss, R. M.; Droudian, A.; Gasser, P.; Shorubalko, I.; Kye, J.-I.; Lee, C.; Park, H. G. Ultimate Permeation Across Atomically Thin Porous Graphene. *Science* **2014**, 344, 289-292.

[25] Qin, L.; Ding, R.; Wang, H.; Wu, J.; Wang, C.; Zhang, C.; Xu, Y.; Wang, L.; Lv, B. Facile synthesis of porous nitrogen-doped holey graphene as an efficient metal-free catalyst for the oxygen reduction reaction. *Nano Res.* **2017**, 10, 305-319.

[26] Duan, H.; Yan, T.; Chen, G.; Zhang, J.; Shi, L.; Zhang, D. A facile strategy for the fast construction of porous graphene frameworks and their enhanced electrosorption performance. *Chem.Commun.* **2017**, 53, 7465-7468.

[27] Viraka Nellore, B. P.; Pramanik, A.; Chavva, S. R.; Sinha, S. S.; Robinson, C.; Fan, Z.; Kanchanapally, R.; Grennell, J.; Weaver, I.; Hamme, A. T.; Ray, P. C. Aptamer-conjugated theranostic hybrid graphene oxide with highly selective biosensing and combined therapy capability. *Faraday Discuss* **2014**, 175, 257-271.

[28] Zhang, Y.; Chen, B.; Zhang, L.; Huang, J.; Chen, F.; Yang, Z.; Yao, J.; Zhang, Z. Controlled assembly of Fe_3O_4 magnetic nanoparticles on graphene oxide. *Nanoscale* **2011**, 3, 1446-1450.

[29] Li, Z.; Zhang, X.; Tan, H.; Qi, W.; Wang, L.; Ali, M. C.; Zhang, H.; Chen, J.; Hu, P.; Fan, C.; Qiu, H. Combustion Fabrication of Nanoporous Graphene for Ionic Separation Membranes. *Adv. Func. Mater.* **2018**, 28, 1805026.

[30] Hummers, W. S.; Offeman, R. E. Preparation of Graphitic Oxide. *J. Am. Chem. Soc.* **1958**, 80, 1339-1339.

[31] Cao, M.; Liu, T.; Gao, S.; Sun, G.; Wu, X.; Hu, C.; Wang, Z. L. Single-Crystal Dendritic Micro-Pines of Magnetic α-Fe_2O_3: Large-Scale Synthesis, Formation Mechanism, and Properties. *Angew. Chem. Int. Ed.* **2005**, 117, 4269-4273.

[32] Liu, Y.; Fu, Y.; Liu, L.; Li, W.; Guan, J.; Tong, G. Low-Cost Carbothermal Reduction Preparation of Monodisperse Fe_3O_4/C Core–Shell Nanosheets for Improved Microwave Absorption. *ACS Appl. Mater. Inter.* **2018**, 10, 16511-16520.

[33] Mi, H.; Yang, X.; Hu, J.; Zhang, Q.; Liu, J. Carbothermal Synthesis of Nitrogen-Doped Graphene Composites for Energy Conversion and Storage Devices. *Front. Chem.* **2018**, 6, 501.

[34] Cheng, W.; Tang, K.; Qi, Y.; Sheng, J.; Liu, Z. One-step synthesis of superparamagnetic monodisperse porous Fe_3O_4 hollow and core-shell spheres. *J. Mater. Chem.* **2010**, 20, 1799-1805.

[35] Bombuwala Dewage, N.; Liyanage, A. S.; Pittman, C. U.; Mohan, D.; Mlsna, T. Fast nitrate and fluoride adsorption and magnetic separation from water on α-Fe_2O_3 and Fe_3O_4 dispersed on Douglas fir biochar. *Bioresource Technol.* **2018**, 263, 258-265.

[36] Allen, M. J.; Tung, V. C.; Kaner, R. B. Honeycomb Carbon: A Review of Graphene. *Chem. Rev.* **2010**, 110, 132-145.

[37] Wan, J.; Huang, L.; Wu, J.; Xiong, L.; Hu, Z.; Yu, H.; Li, T.; Zhou, J. Microwave Combustion for Rapidly Synthesizing Pore-Size-Controllable Porous Graphene. *Adv. Func. Mater.* **2018**, 28, 1800382.

[38] Jiang, H.-B.; Zhang, Y.-L.; Zhang, Y.; Liu, Y.; Fu, X.-Y.; Liu, Y.-Q.; Wang, C.-D.; Sun, H.-B. Flame treatment of graphene oxides: cost-effective production of nanoporous graphene electrode for Lithium-ion batteries. *Sci. Rep.* **2015**, 5, 17522.

[39] Zhang, H.-j.; Qi, S.-d.; Niu, X.-y.; Hu, J.; Ren, C.-l.; Chen, H.-l.; Chen, X.-g. Metallic nanoparticles immobilized in magnetic metal–organic frameworks: preparation and application as highly active, magnetically isolable and reusable catalysts. *Catal. Sci. Tech.* **2014**, 4, 3013-3024.

[40] Zhang, H.; Chen, Y.; Liang, M.; Xu, L.; Qi, S.; Chen, H.; Chen, X. Solid-Phase Synthesis of Highly Fluorescent Nitrogen-Doped Carbon Dots for Sensitive and Selective Probing Ferric Ions in Living Cells. *Anal. Chem.* **2014**, 86, 9846-9852.

[41] Zhang, H.; Zhang, B.; Di, C.; Ali, M. C.; Chen, J.; Li, Z.; Si, J.; Zhang, H.; Qiu, H. Label-free fluorescence imaging of cytochrome c in living systems and anti-cancer drug screening with nitrogen doped carbon quantum dots. *Nanoscale* **2018**, 10, 5342-5349.

[42] Li, Y.; Zhang, R.; Tian, X.; Yang, C.; Zhou, Z. Facile synthesis of Fe_3O_4 nanoparticles decorated on 3D graphene aerogels as broad-spectrum sorbents for water treatment. *Appl. Surf. Sci.* **2016**, 369, 11-18.

[43] Combellas, C.; Delamar, M.; Kanoufi, F.; Pinson, J.; Podvorica, F. I. Spontaneous Grafting of Iron Surfaces by Reduction of Aryldiazonium Salts in Acidic or Neutral Aqueous Solution. Application to the Protection of Iron against Corrosion. *Chem. Mater.* **2005**, 17, 3968-3975.

[44] Grosvenor, A. P.; Kobe, B. A.; Biesinger, M. C.; McIntyre, N. S. Investigation of multiplet splitting of Fe 2p XPS spectra and bonding in iron compounds. *Surf. Interf. Anal.* **2004**, 36, 1564-1574.

[45] An, Q.; Lv, F.; Liu, Q.; Han, C.; Zhao, K.; Sheng, J.; Wei, Q.; Yan, M.; Mai, L. Amorphous Vanadium Oxide Matrixes

Supporting Hierarchical Porous Fe_3O_4/Graphene Nanowires as a High-Rate Lithium Storage Anode. *Nano Lett.* **2014**, 14, 6250-6256.

[46] Tao, Y.; Lin, Y.; Huang, Z.; Ren, J.; Qu, X. Incorporating Graphene Oxide and Gold Nanoclusters: A Synergistic Catalyst with Surprisingly High Peroxidase-Like Activity Over a Broad pH Range and its Application for Cancer Cell Detection. *Adv. Mater.* **2013**, 25, 2594-2599.

[47] Dong, Y.-l.; Zhang, H.-g.; Rahman, Z. U.; Su, L.; Chen, X.-j.; Hu, J.; Chen, X.-g. Graphene oxide–Fe_3O_4 magnetic nanocomposites with peroxidase-like activity for colorimetric detection of glucose. *Nanoscale* **2012**, 4, 3969-3976.

[48] Tan, H.; Li, Q.; Zhou, Z.; Ma, C.; Song, Y.; Xu, F.; Wang, L. A sensitive fluorescent assay for thiamine based on metal-organic frameworks with intrinsic peroxidase-like activity. *Anal. Chim. Acta* **2015**, 856, 90-95.

[49] Hatel, R.; Goumri, M.; Ratier, B.; Baitoul, M. Graphene derivatives/Fe_3O_4/polymer nanocomposite films: Optical and electrical properties. *Mater. Chem. Phys.* **2017**, 193, 156-163.

[50] Qiao, F.; Qi, Q.; Wang, Z.; Xu, K.; Ai, S. MnSe-loaded g-C_3N_4 nanocomposite with synergistic peroxidase-like catalysis: Synthesis and application toward colorimetric biosensing of H_2O_2 and glucose. *Sens. Actuat. B* **2016**, 229, 379-386.

[51] Yadav, S. V.; Rathod, V. K. Enzyme mimic oxidase-like activity of Fe_3O_4 magnetic nanoparticles for dopamine detection. *Catal. Green Chem. Eng.* **2018**, 1, 357-368.

[52] Jin, L.-Y.; Dong, Y.-M.; Wu, X.-M.; Cao, G.-X.; Wang, G.-L. Versatile and Amplified Biosensing through Enzymatic Cascade Reaction by Coupling Alkaline Phosphatase in Situ Generation of Photoresponsive Nanozyme. *Anal. Chem.* **2015**, 87, 10429-10436.

[53] Du, J.; Wang, J.; Huang, W.; Deng, Y.; He, Y. Visible Light-Activatable Oxidase Mimic of 9-Mesityl-10-Methylacridinium Ion for Colorimetric Detection of Biothiols and Logic Operations. *Anal. Chem.* **2018**, 90, 9959-9965.

[54] Liu, L.; Sun, C.; Yang, J.; Shi, Y.; Long, Y.; Zheng, H. Fluorescein as a Visible-Light-Induced Oxidase Mimic for Signal-Amplified Colorimetric Assay of Carboxylesterase by an Enzymatic Cascade Reaction. *Chem. Eur. J.* **2018**, 24, 6148-6154.

[55] Wefers, H.; Sies, H. Oxidation of glutathione by the superoxide radical to the disulfide and the sulfonate yielding singlet oxygen. *Eur. J. Biochem.* **1983**, 137, 29-36.

[56] Zhu, W.; Chi, M.; Gao, M.; Wang, C.; Lu, X. Controlled synthesis of titanium dioxide/molybdenum disulfide core-shell hybrid nanofibers with enhanced peroxidase-like activity for colorimetric detection of glutathione. *J. Colloid Interf. Sci.* **2018**, 528, 410-418.

[57] Liu, J.; Meng, L.; Fei, Z.; Dyson, P. J.; Jing, X.; Liu, X. MnO_2 nanosheets as an artificial enzyme to mimic oxidase for rapid and sensitive detection of glutathione. *Biosens. Bioelectron.* **2017**, 90, 69-74.

[58] Feng, J.; Huang, P.; Shi, S.; Deng, K.-Y.; Wu, F.-Y. Colorimetric detection of glutathione in cells based on peroxidase-like activity of gold nanoclusters: A promising powerful tool for identifying cancer cells. *Anal. Chim. Acta* **2017**, 967, 64-69.

[59] Qi, S.; Liu, W.; Zhang, P.; Wu, J.; Zhang, H.; Ren, H.; Ge, J.; Wang, P. A colorimetric and ratiometric fluorescent probe for highly selective detection of glutathione in the mitochondria of living cells. *Sensor. Actuat. B* **2018**, 270, 459-465.

[60] Du, T.; Zhang, H.; Ruan, J.; Jiang, H.; Chen, H.-Y.; Wang, X. Adjusting the Linear Range of Au-MOF Fluorescent Probes for Real-Time Analyzing Intracellular GSH in Living Cells. *ACS Appl. Mater. Inter.* **2018**, 10, 12417-12423.

[61] Yang, R.; Guo, X.; Jia, L.; Zhang, Y. A fluorescent "on-off-on" assay for selective recognition of Cu(II) and glutathione based on modified carbon nanodots, and its application to cellular imaging. *Microchim. Acta* **2017**, 184, 1143-1150.

[62] Zhang, Y.; Shao, X.; Wang, Y.; Pan, F.; Kang, R.; Peng, F.; Huang, Z.; Zhang, W.; Zhao, W. Dual emission channels for sensitive discrimination of Cys/Hcy and GSH in plasma and cells. *Chem. Commun.* **2015**, 51, 4245-4248.

[63] Li, H.; Peng, W.; Feng, W.; Wang, Y.; Chen, G.; Wang, S.; Li, S.; Li, H.; Wang, K.; Zhang, J. A novel dual-emission fluorescent probe for the simultaneous detection of H_2S and GSH. *Chem. Commun.* **2016**, 52, 4628-4631.

Table of Content